arXiv:nucl-th/0610037v1 10 Oct 2006

# Microscopic three-body forces and kaon condensation in cold neutrino-trapped matter

A. Li[1], G. F. Burgio[2], U. Lombardo[3], W. Zuo[1]

[1] *School of Physical Science and Technology, Lanzhou University,*
*and Institute of Modern Physics, Chinese Academy of Sciences, Lanzhou 730000, P. R. China*
[2] *INFN Sezione di Catania, Via Santa Sofia 64, I-95123 Catania, Italy*
[3] *INFN-LNS, Via Santa Sofia 44, I-95123 Catania, and Department of Physics and Astrophysics,*
*Catania University, Via Santa Sofia 64, I-95123, Italy*

(Dated: February 5, 2008)

We investigate the composition and the equation of state of the kaon condensed phase in neutrino-free and neutrino-trapped star matter within the framework of the Brueckner-Hartree-Fock approach with three-body forces. We find that neutrino trapping shifts the onset density of kaon condensation to a larger baryon density, and reduces considerably the kaon abundance. As a consequence, when kaons are allowed, the equation of state of neutrino-trapped star matter becomes stiffer than the one of neutrino free matter. The effects of different three-body forces are compared and discussed. Neutrino trapping turns out to weaken the role played by the symmetry energy in determining the composition of stellar matter, and thus reduces the difference between the results obtained by using different three-body forces.

PACS numbers: 21.65.+f, 26.60.+c, 24.10.Cn, 97.60.Jd, 13.75.Cs

## I. INTRODUCTION

Within a newly born neutron star or proto-neutron star (PNS) neutrinos are temporarily trapped in a time scale of several tens of seconds, which would undoubtedly contribute to the overall chemical equilibrium, and may change the structure and composition of the star. Neutrino trapping is expected to have a strong influence on the equation of state (EOS) of $\beta$-stable neutron star matter [1], and, as a consequence, affects the theoretical predictions of the maximum mass and the corresponding radius. The EOS of the neutrino trapped stellar matter is particularly important for the evolution of a newly born neutron star and the mechanism of black hole formation. The effects of neutrino trapping in stellar matter and its implications for astrophysical phenomena were explored by several authors [1, 2, 3, 4, 5, 6, 7]. In Ref.[1], Prakash et al. investigated systematically the structure and composition of PNSs by using various theoretical models including the schematic potential model [8], the relativistic field approach [9] based on the Walecka model [10], and the effective chiral model [11]. It was argued that a black hole would be most likely formed in a neutrino diffusion timescale of $\approx 10$ s, if the maximum mass of the hot neutrino-trapped star is about $1.5M_\odot$ in presence of negatively-charged hadrons. In Ref.[4, 7], the presence of neutrinos was shown to delay the onset of hyperons, thus changing significantly the composition of star matter, and making the EOS stiffer. In Ref. [3], the evolution of PNSs with quarks was explored.

In the interior of a neutron star (NS) or PNS, the baryon density could be as high as several times the value of the nuclear matter saturation density, and thus the matter is expected to become exotic. Among the possible exotic phases in dense nuclear matter, the kaon condensation is a subject of great interest in nuclear physics, hadronic physics and neutron star physics [11, 12, 13, 14, 15]. The presence of a kaon condensation may have important consequences for determining structure [16, 17, 18, 19], cooling rates [20, 21, 22, 23] and evolution of neutron stars [24]. The phase transition from normal matter to the kaon condensed matter is also expected to affect the transport properties and the glitch behavior of pulsars [25]. Other strange phases could also appear in competition or coexisting with kaons; in particular, hyperons are expected to occur at $2-3$ times the saturation density [1], before the onset of kaon condensation.

In Ref.[26], the effects of different three-body forces on the neutron star maximum mass were investigated within the Brueckner-Hartree-Fock (BHF) approach. In Ref.[27], the kaon condensation in neutrino-free NS matter was studied in the same theoretical approach. It was found that the composition of NS matter is sensitively dependent on the nuclear symmetry energy and the presence of kaons. In the present paper we shall extend the previous work to the study of neutrino trapped matter at zero temperature, focussing particularly on the interplay between the roles played by TBFs, neutrino trapping and kaon condensation. Effects due to finite temperature, which are important for the internal composition of protoneutron stars, and their evolution [3, 17, 28, 29], will be discussed within the Brueckner-Hartree-Fock approach, in a subsequent paper[30]. .

The present paper is organized as follows. In Sect.2 we review briefly the theoretical models adopted in our calculations, i.e., the BHF approach, and the chiral model for kaon-nucleon interaction. In Sect.3 we discuss the stellar matter composition both with and without neutrino trapping, and the resulting EOS. Our numerical results are presented in Sect.4. Finally, a summary is given in Sect.5.

## II. THEORETICAL MODELS

### A. Brueckner-Bethe-Goldstone theory

In the present work, we employ the Brueckner approach for asymmetric nuclear matter [31, 32] to calculate the baryonic contribution to the EOS of the stellar matter. The starting point of the BHF approach is the interaction $G$ matrix which satisfies the Brueckner-Bethe-Goldstone (BBG) equation[31, 32]

$$G(\rho, x_p; \omega) = v_{NN} + v_{NN} \sum_{k_1 k_2} \frac{|k_1 k_2\rangle Q \langle k_1 k_2|}{\omega - \epsilon(k_1) - \epsilon(k_2)} G(\rho, x_p; \omega), \tag{1}$$

where $\omega$ is the starting energy, and $x_p = \rho_p/\rho$ is the proton fraction, being $\rho_p$, and $\rho$ the proton and the total baryon density, respectively. $Q$ is the Pauli operator, which prevents the two intermediate nucleons from being scattered into the states below the Fermi sea, and $\epsilon(k)$ is the single particle energy given by $\epsilon(k) \equiv \epsilon(k;\rho) = \hbar^2 k^2/(2m) + U(k;\rho)$. The single particle potential $U(k)$ is calculated from the real part of the on-shell $G$-matrix and we adopt for it the so called *continuous choice* [33], i.e. for any momentum $k$ below and above the Fermi surface

$$U(k;\rho) = \mathrm{Re} \sum_{k' \leq k_F} \langle kk'|G[\rho; e(k) + e(k')]|kk'\rangle_a, \tag{2}$$

where the subscript "$a$" indicates antisymmetrization of the matrix element. Due to the occurrence of $U(k)$ in Eqs. (1) and (2), the latter constitute a coupled system of equations that has to be solved in a self-consistent way. In the BHF approximation the energy per nucleon is

$$\frac{E}{A} = \frac{3}{5}\frac{k_F^2}{2m} + \frac{1}{2\rho} \sum_{k,k' \leq k_F} \langle kk'|G[\rho; e(k) + e(k')]|kk'\rangle_a. \tag{3}$$

Adopting the continuous choice for the single-particle potential, the two hole-line (BHF) truncation of the energy shift turns out to be a good approximation for the nuclear EOS, since the results in this scheme are quite close to those obtained by including also the three hole-line contribution [34]. The basic input of the BBG equation is the realistic baryon-baryon interaction, which is determined by reproducing the nucleon-nucleon scattering phase shifts. The realistic nucleon-nucleon (NN) interaction $v_{NN}$ adopted in the present calculation is the Argonne $v_{18}$ two-body force [35]. Since nonrelativistic calculations, based on purely two-body interactions, fail to reproduce the correct saturation point of symmetric nuclear matter, three-body forces (TBFs) among nucleons are usually introduced [36]. They turn out to be needed to correct this deficiency. In this work two models have been used, i.e., the phenomenological Urbana model [37], and a microscopic TBF constructed from the meson-exchange current approach [38]. In both cases, the BBG approach is applicable only if the TBF is reduced to an effective two body force, which has to be added to the bare two body interaction. This is done by averaging over the position of the third particle, assuming that the probability of having two particles at a given distance is given by the two-body correlation function. The resulting potential is a density dependent two-body force [36]. The inclusion of the microscopic TBF in the calculation for asymmetric nuclear matter has been performed in Ref. [39].

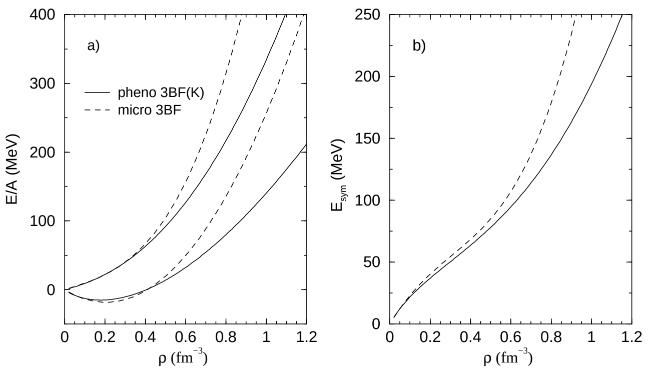

FIG. 1: The EoS is shown (panel (a)) for symmetric (lower curves) and pure neutron matter (upper curves). The symmetry energy as a function of the nucleon density is displayed in panel (b). See text for details.

In Fig.1, panel a), we show the equation of state for symmetric nuclear matter (lower curves) and pure neutron matter (upper curves). The solid lines represent the values obtained using the Urbana phenomenological TBF, whereas the dashed lines are the values obtained by adopting the microscopic TBF. We notice that the results of the two adopted TBFs show a similar behavior up to density $\rho \approx 0.4\ fm^{-3}$, but they differ a lot in the high density range. In particular, the microscopic TBF turns out to be more repulsive than the Urbana model at high densities, and the discrepancy between the two predictions becomes increasingly large as the density increases.

Nucleonic TBFs play an essential role in determining the chemical composition of a neutron star. In fact, as shown below, the baryon chemical potentials and the symmetry energy strongly depend on the choice of TBFs, for densities typical of those encountered in the neutron star cores. The proton and neutron chemical potentials can be derived from the energy density through the standard thermodynamic relation

$$\mu_{p,n} = (\partial\varepsilon/\partial\rho_{p,n})_{\rho_i}, \tag{4}$$

with all remaining densities $\rho_i$ fixed. In asymmetric nuclear matter, the calculation involves the knowledge of the energy per particle and its partial derivatives with respect to the total baryon density and proton fraction, i.e.

$$\mu_n(\rho, x_p) = E/A + \rho\frac{\partial E/A}{\partial \rho} - x_p\frac{\partial E/A}{\partial x_p} \tag{5}$$

$$\mu_p(\rho, x_p) = E/A + \rho\frac{\partial E/A}{\partial \rho} + (1-x_p)\frac{\partial E/A}{\partial x_p} \tag{6}$$

Actually, the energy per particle $E/A$ may be expanded quadratically in the proton concentration $x_p$ about its value for symmetric matter ($x_p = \frac{1}{2}$):

$$\frac{E}{A}(\rho, x_p) = \frac{E}{A}(\rho, \frac{1}{2}) + (1-2x_p)^2 E_{sym} + \mathcal{O}((1-2x_p)^4) \tag{7}$$

Microscopic investigations [8, 31, 32] have shown that the expansion up to the quadratic term is a good approximation and the higher-order contributions is negligible. As a consequence, the difference of the neutron and proton chemical potentials is determined by the symmetry energy in an explicit way

$$\mu_n - \mu_p = 4(1-2x_p)E_{sym}(\rho) \tag{8}$$

which implies that the symmetry energy plays a decisive role in predicting the chemically equilibrated compositions of PNSs and NSs.

In Fig.1, panel b), we show the symmetry energy calculated in the BHF approach as a function of the nucleon density. Its value at the normal nuclear matter density has been well determined to be 30 ± 4 MeV. Actually, the calculations performed with either the Urbana phenomenological TBF (solid line) or the microscopic TBF (dashed line) reproduce correctly this value. However, the high density behavior suffers a large uncertainty, and this reflects in the theoretical predictions of the neutron star composition. Moreover, we see that the symmetry energy predicted by using the microscopic TBF rises much faster at high densities than the one obtained by adopting the phenomenological TBF.

As far as leptons are concerning, the energies and chemical potentials are obtained by solving the free Fermi gas model at zero temperature [40]. Once the baryonic and leptonic chemical potentials are known, one can proceed to calculate the composition of the $\beta$-stable stellar matter, and then the total energy per particle $(E/A)_{tot}$ and pressure $P$ through the usual thermodynamical relation

$$P = \rho^2\frac{d(E/A)_{tot}}{d\rho} \tag{9}$$

### B. Kaon condensation

In the present paper, we use the effective chiral theory proposed by Kaplan and Nelson [11] and extensively investigated afterwards [41]. In this model, the $SU(3)\times SU(3)$ chiral Lagrange density is expressed as

$$\begin{aligned}\mathcal{L}_\chi = {} & \frac{f^2}{4}\mathrm{Tr}\partial_\mu U\partial^\mu U^\dagger + \mathrm{Tr}\bar{B}(i\gamma^\mu D_\mu - m_B)B \\ & + F\,\mathrm{Tr}\bar{B}\gamma^\mu\gamma_5[\mathcal{A}_\mu, B] + D\,\mathrm{Tr}\bar{B}\gamma^\mu\gamma_5\{\mathcal{A}_\mu, B\} \\ & + c\mathrm{Tr}\mathcal{M}(U+U^\dagger) + a_1\mathrm{Tr}\bar{B}(\xi\mathcal{M}\xi + \xi^\dagger\mathcal{M}\xi^\dagger)B \\ & + a_2\mathrm{Tr}\bar{B}B(\xi\mathcal{M}\xi + \xi^\dagger\mathcal{M}\xi^\dagger) \qquad (10) \\ & + a_3\mathrm{Tr}\bar{B}B\,\mathrm{Tr}(\xi\mathcal{M}\xi + \xi^\dagger\mathcal{M}\xi^\dagger). \qquad (11)\end{aligned}$$

The first four terms conserve the chiral symmetry, and the other terms break the chiral symmetry. Parameters in the symmetric part are $f = 93$ MeV, the pion decay constant, $D = 0.81$, and $F = 0.44$. The breaking strength is determined by the parameters $a_1, a_2, a_3$, and $c$, as well as by the quark mass matrix $\mathcal{M}$. We adopt $a_1 m_s = -67$ MeV and $a_2 m_s = 134$ MeV, as determined from the baryon mass splittings [42]. The constant $c$ and the bare kaon mass are related by the Gell-Mann-Oakes-Renner relation $m_K^2 = 2cm_s/f^2$. The parameter $a_3 m_s$ had remained largely uncertain for many years, due to our poor knowledge of the strangeness content of the proton and the kaon-nucleon sigma term $\Sigma_{KN}$ [11, 12, 42, 43]. Fortunately, the large ambiguity in this parameter has been settled recently by Dong, Lagaë and Liu [44] with small error based on the lattice calculations. In the present calculations we adopt values of $a_3 m_s$ equal to $-310, -222, \text{and} -134$ MeV, as done in Refs.[16, 23], in order to investigate the sensitivity of our results to the variation of the proton strangeness content. Our adopted central value $a_3 m_s = -222$ MeV is very close to the value extracted from the lattice gauge calculations in Ref. [44], which is $-231$ MeV with error of less than 4%. The value of $a_3 m_s$ is essential in determining the onset density for kaon condensation, since it provides the attractive component of the kaon-nucleon interaction.

In principle, the chiral Lagrangian should give the EoS of baryons and mesons, but so far only the kaon-nucleon interaction has been extracted from it. Therefore, we use the chiral Lagrangian only to extract the kaon-nucleon part of the interactions, and take the EoS for nuclear matter from the Brueckner many-body theory. This means that the energy density is a sum of three contributions: the kaon-nucleon interaction energy density (derived from $\mathcal{L}_\chi$), the nucleon-nucleon energy density, and the energy density for leptons $(e, \mu)$:

$$\epsilon = \epsilon_{KN} + \epsilon_{NN} + \epsilon_{lep}. \tag{12}$$

From eq.(7), we get the nucleon-nucleon contribution as

$$\epsilon_{NN}(\rho, x_p) = \rho\frac{E}{A}(\rho, x_p), \tag{13}$$

whereas the energy density for leptons is the one for a free Fermi gas at zero temperature, and can be found in textbooks [40].

Following exactly the standard prescription in Ref. [16], we can get the kaon-nucleon energy density of the kaon condensed matter from applying the Baym theorem [45], i.e.

$$\epsilon_{KN} = \frac{f^2}{2}\mu_K^2\sin^2\theta + 2m_K^2 f^2\sin^2\frac{\theta}{2} \tag{14}$$

$$+ \;\; \rho(2a_1 x_p + 2a_2 + 4a_3) m_s \sin^2 \frac{\theta}{2} \qquad (15)$$

where $\rho$ and $x_p$ denote the nucleon number density and the proton fraction, respectively, and $\theta$ is the amplitude of the condensation. We remind the reader that in this work we neglect the effects of $\bar{K}^0$ condensation, which could play a significant role at the high densities typical of neutron star cores, as it has been shown in Ref.[18, 19].

## III. EQUATION OF STATE OF COLD CATALYZED STELLAR MATTER

For stars in which the strongly interacting particles are only baryons, the chemical composition is determined by the requirements of charge neutrality and equilibrium under the weak processes

$$B_1 \to B_2 + l + \bar{\nu}_l, \quad B_2 + l \to B_1 + \nu_l \qquad (16)$$

where $B_1$ and $B_2$ are baryons, $l$ denotes a lepton, either an electron or a muon, and $\nu_l(\bar{\nu}_l)$ a (anti-)neutrino. Under the condition of neutrino escape, these two requirements imply that the relations

$$\sum_i q_i x_i + \sum_l q_l x_l = 0 \qquad (17)$$

$$\mu_i = b_i \mu_n - q_i \mu_l \qquad (18)$$

are satisfied. In the above expression, $x_i = \rho_i/\rho_B$ represents the baryon fraction for the species $i$, and $\rho_B$ the baryon density. The neutron chemical potential is denoted by $\mu_n$, whereas $\mu_i$ refers to the chemical potential of the baryon species $i$, $b_i$ to its baryon number and $q_i$ to its electric charge. The same notation holds true for those quantities with subscript $l$, i.e. leptons. Under condition when the neutrinos are trapped in the system, the beta equilibrium condition (18) is altered to

$$\mu_i = b_i \mu_n - q_i(\mu_l - \mu_{\nu_l}) \qquad (19)$$

where $\mu_{\nu_l}$ is the chemical potential of the neutrino $\nu_l$.

Because of the trapping, the numbers of leptons per baryon of each flavor of neutrino $l = e, \mu$,

$$Y_{L_l} = x_l + x_{\nu_l}, \qquad (20)$$

are conserved on dynamical time scales. Gravitational collapse calculations of the white-dwarf core of massive stars indicate that at the onset of trapping, the electron lepton number $Y_{L_e} = x_e + x_{\nu_e} \simeq 0.4$, the precise value depending on the efficiency of electron capture reactions during the initial collapse stage. Also, because no muons are present when neutrinos become trapped, the constraint $Y_{L_\mu} = x_\mu + x_{\nu_\mu} = 0$ can be imposed. We fix $Y_{L_l}$ at these values in our calculations for neutrino trapped matter.

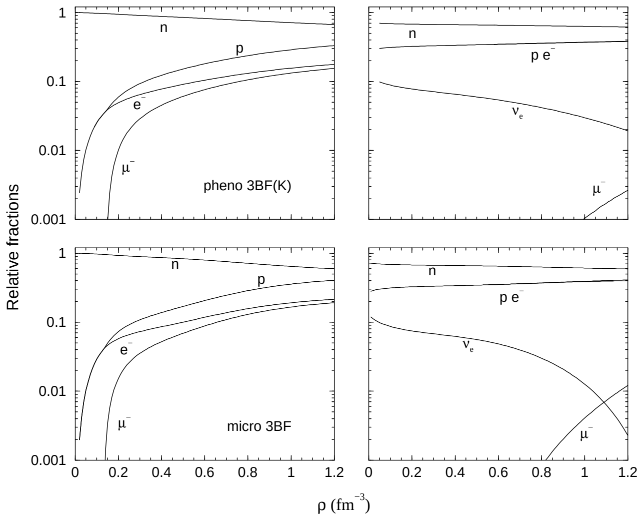

FIG. 2: The particle populations are shown as a function of the nucleon density for neutrino free (left hand panels) and neutrino trapped matter (right hand panels). In the upper (lower) panels results are displayed for the case when the phenomenological Urbana (microscopic) TBF is used.

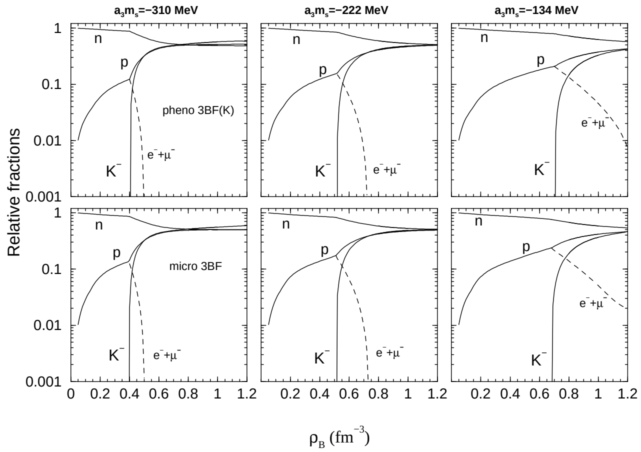

FIG. 3: The particle populations are shown as a function of the baryon density for neutron star matter with kaons, for three different values of $a_3 m_s$. In the upper (lower) panels results are displayed for the case when the phenomenological Urbana (microscopic) TBF is used.

In the neutron star matter with kaons the chemical equilibrium can be reached through the following reactions

$$n \leftrightarrow p + l + \nu_l, \quad n \leftrightarrow p + K^-, \quad l \leftrightarrow K^- + \nu_l, \qquad (21)$$

where $l$ denotes leptons, i.e., $l = e, \mu$. One can determine the ground state by minimizing the total energy density with respect to the condensate amplitude $\theta$ keeping all densities fixed. This minimization together with the chemical equilibrium and charge neutrality conditions leads to the following three coupled equations [16, 23]

$$\begin{aligned}\cos\theta &= \frac{1}{f^2\mu^2}[m_K^2 f^2 + \frac{1}{2}u\rho_0(2a_1x_p+2a_2+4a_3)m_s \qquad (22)\\ &- \frac{1}{2}\mu u\rho_0(1+x_p)], \qquad (23)\end{aligned}$$

and

$$\begin{aligned}\mu &\equiv \mu_e - \mu_{\nu_e} = \mu_K = \mu_n - \mu_p \qquad (24)\\ &= 4(1-2x_p)S(u)\sec^2\frac{\theta}{2} - 2a_1 m_s\tan^2\frac{\theta}{2}\,, \qquad (25)\end{aligned}$$

$$\begin{aligned}&f^2\mu\sin^2\theta + u\rho_0(1+x_p)\sin^2\frac{\theta}{2} - x_p u\rho_0 \qquad (26)\\ &+\frac{{\mu_e}^3}{3\pi^2} + \eta(|\mu| - m_\mu)\frac{(\mu_\mu^2 - m_\mu^2)^{3/2}}{3\pi^2} = 0, \qquad (27)\end{aligned}$$

where $u \equiv \rho_B/\rho_0$ is the baryon number density in units of $\rho_0$. The last two equations are from the chemical equilibrium and charge neutrality conditions, respectively. For the neutrino-free case, the above equations recover the ones given in Ref.[27]. The EOS and the composition of the kaon condensed phase in the chemically equilibrated neutron star matter can be obtained by solving the coupled equations (23), (25), and (27). The critical density for kaon condensation is determined as the point above which a real solution for the coupled equations can be found.

The stable configurations of a neutron star can be obtained from the well known hydrostatic equilibrium equations of Tolman, Oppenheimer and Volkoff [40, 46, 47] for the pressure $P$ and the enclosed mass $m$

$$\frac{dP(r)}{dr} = -\frac{Gm(r)\mathcal{E}(r)}{r^2}\frac{\left[1+\frac{P(r)}{\mathcal{E}(r)}\right]\left[1+\frac{4\pi r^3 P(r)}{m(r)}\right]}{1-\frac{2Gm(r)}{r}}, \quad (28)$$

$$\frac{dm(r)}{dr} = 4\pi r^2\mathcal{E}(r), \quad (29)$$

once the equation of state $P(\mathcal{E})$ is specified, being $\mathcal{E}$ the total energy density ($G$ is the gravitational constant). For a chosen central value of the energy density, the numerical integration of Eqs.(28, 29) provides the mass-radius relation. For the description of the NS's crust, we have joined the hadronic equations of state above described with the ones by Negele and Vautherin [48] in the medium-density regime ($0.001\ fm^{-3} < \rho < 0.08\ fm^{-3}$), and the ones by Feynman-Metropolis-Teller [49] and Baym-Pethick-Sutherland [50] for the outer crust ($\rho < 0.001\ fm^{-3}$).

## IV. RESULTS AND DISCUSSION

In Fig. 2 we present the composition of the $\beta$-equilibrated neutrino-free (left-hand panels) and neutrino-trapped $npe\mu$ matter (right-hand panels). The upper panels display results obtained using the Argonne $v_{18}$ two-body potential supplemented by the phenomenological Urbana TBF, whereas in the lower panels we show the populations obtained when the microscopic TBFs are used. In the neutrino-free case, we notice that a stiffer symmetry energy produces a larger proton concentration in the region $\rho \geq 0.6\ fm^{-3}$, where the proton fraction $x_p \approx E_{sym}^3$. In neutrino-trapped matter, the lepton concentration becomes sizeably higher because the electron chemical potential must keep at a high value, in order to fulfill the $\beta$-equilibrium condition. This leads to a larger proton fraction as compared to the neutrino-free case, because of the charge neutrality. Therefore, neutrino-trapped matter is more symmetric than the neutrino-free one.

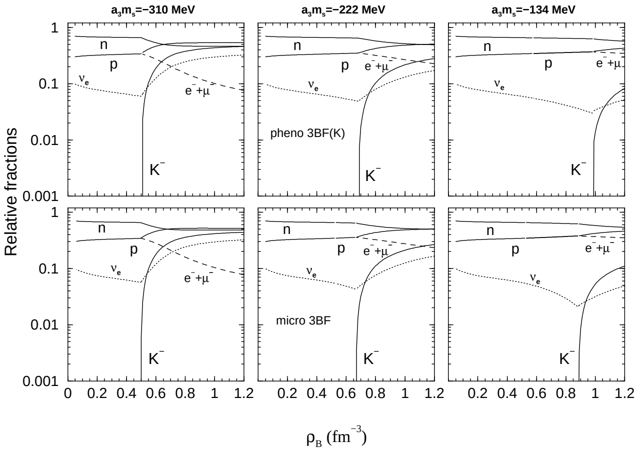

FIG. 4: Same as Fig. 3, but for neutrino trapped matter.

We also notice that the differences in proton populations, due to the different TBFs adopted, are smoothed out when neutrinos are trapped. This is readily understood as follows. In neutrino-free matter, the electron chemical potential is determined mainly by the density dependence of nuclear symmetry energy. When neutrinos are trapped, they contribute to the chemical equilibrium, and, as a consequence, the electron chemical potential is determined simultaneously by the neutrino trapping effect and by the symmetry energy. Because of the lepton number conservation, the major effect of trapping is to keep the electron concentration high, and this reduces considerably the role played by the symmetry energy in determining the star composition.

Let us now discuss the case when kaons are present in $\beta$ stable and neutrally charged matter. In Fig. 3 we show the particle fractions for neutrino free star matter, using alternatively the phenomenological Urbana TBF (upper panels) and the microscopic one (lower panels). We have chosen three different values of the parameter $a_3m_s$, respectively $a_3m_s = -310, -222, \text{and} -134$ MeV. We observe that the kaon threshold depends sensitively on the attraction term of the kaon-nucleon interaction. In the extreme case of $a_3m_s = -310$ MeV, the predicted kaon onset density is the lowest, of the order of 0.4 $\mathrm{fm}^{-3}$, almost independently on the adopted nucleonic TBF. This is due to the fact that, up to densities of the order of 0.6 $\mathrm{fm}^{-3}$, both kinds of TBF produce a very similar symmetry energy. In addition, the role played by the kaon-nucleon interaction becomes more predominant over that by the symmetry energy for a stronger kaon-nucleon interaction term. For larger densities, the microscopic TBF gives a higher symmetry energy, and this leads to a slightly different kaon threshold when a weak attractive term is adopted. We also notice a dramatic decrease of the lepton population and increase of the proton concentration as a consequence of the kaon appearance. This is due to the charge neutrality condition, which has to be always fulfilled. We notice that the threshold densities for kaon condensation may be delayed by the onset of hyperons, as found by other authors [19, 51, 52].

In Fig.4 the particle population is plotted as a function of the baryon density for the neutrino trapped case. We notice that, because of trapped neutrinos, the onset of kaon condensation is shifted to larger densities than in neutrino free matter. Even in that case, both TBF's produce very similar results, except for the less attractive case, i.e. $a_3 m_s = -134$ MeV, where the onset for kaon condensation takes place at a lower density for the microscopic TBF. This is due to the fact that, at high density, the symmetry energy is larger, and this allows for a kaon condensed phase at baryon density lower than in the case with the Urbana TBF. As compared to the neutrino free case, the kaon abundance in the condensed phase is much smaller than in neutrino trapped matter, due to the larger electron population. In contrast to the normal phase, in the condensed phase the number of neutrinos rises up as the baryon density increases, and this is because the presence of kaons leads to a decrease of the electron population as a function of the baryon density. We notice that the values of the threshold densities for $K^-$ condensation both in neutrino-free and neutrino-trapped matter are in very good agreement with those found in ref.[1]. However, the threshold densities are dependent both on the value of the temperature, and the attraction term of the kaon-nucleon interaction [1, 3].

Once the relative particle concentrations are known, we can calculate the equation of state. This is shown in Fig.5, both for the neutrino free case (upper panels), and the neutrino trapped one (lower panels). In the case without kaons, the equation of state of neutrino trapped matter is slightly softer than the neutrino free one, because the loss in energy due to the reduction of the neutron-proton asymmetry as a consequence of the increase of the proton abundance exceeds the gain from the presence of neutrinos [1]. We observe that the kaon condensation produces a general softening of the equation of state with respect to the purely nucleonic case. The degree of softening depends on the value of the parameter $a_3 m_s$, i.e., the larger the value of $|a_3 m_s|$ the stronger the softening is. In the case with kaon condensate, neutrino trapping produces a stiffer equation of state due to the higher onset density of kaons and smaller kaon abundance, as shown in Fig.4. It is evident from the figure that the softening of the equation of state due to kaon condensate is much less pronounced in neutrino trapped matter than in neutrino free matter. This may lead a newly-formed, hot protoneutron star to metastability, i.e. a delayed collapse while cooling down, as discussed in ref.[1, 17].

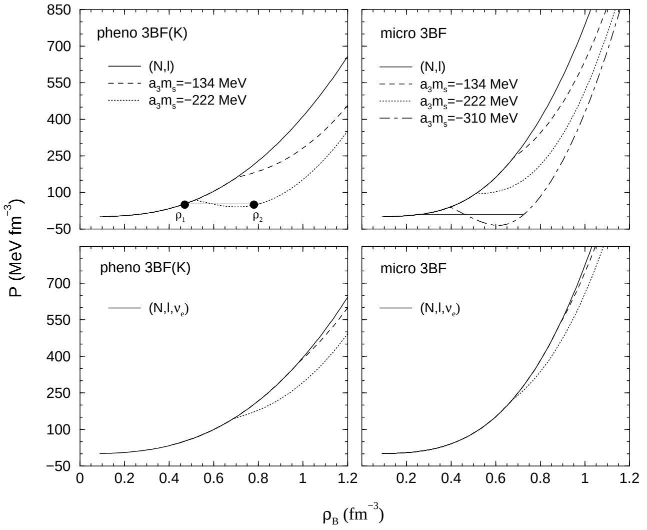

FIG. 5: The pressure for beta-equilibrated neutrino free (upper panels) and neutrino trapped matter (lower panels) is shown as a function of the baryon density, for phenomenological (left-hand side) and microscopic TBF's (right-hand side). The thin solid lines represent the Maxwell construction.

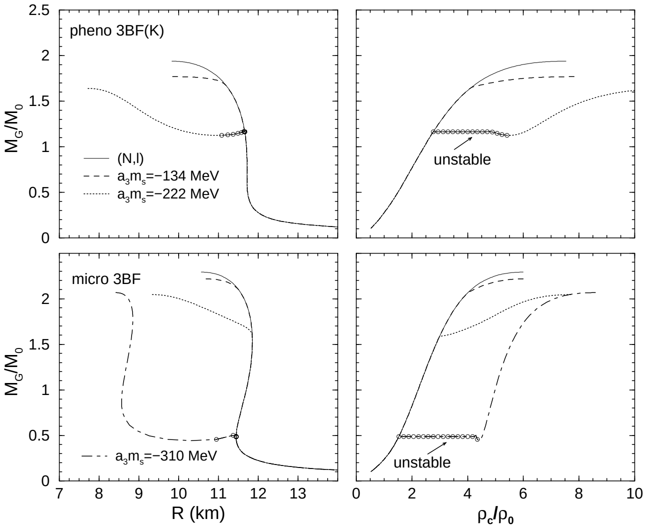

FIG. 6: The gravitational mass is shown as a function of the radius (left-hand side) and the normalized central density (right hand side), for the phenomenological (upper panels) and microscopic TBF's (lower panels) in neutrino free matter. Circles represent unstable configurations.

In some cases, the onset of a kaon condensed phase produces a negative compressibility in the equation of state.

Following Migdal [53], we have performed a Maxwell construction to maintain a positive compressibility. We should note that the Maxwell construction is valid for substances with only one independent component. Neutron star matter has two independent components (the baryon and electric charge). Therefore, the Maxwell construction cannot satisfy Gibbs' criteria that pressure, temperature and all chemical potentials be common to both phases in equilibrium. A novel treatment of the phase transition in $\beta$ stable matter has been proposed by Glendenning[54] for the hadron-quark phase transition, and has been subsequently extended to the study of the kaon condensed phase, treated as a first order phase transition in neutron star matter [25]. The Gibbs construction has strong consequences on the mechanical stability of neutron stars, because the pressure is a monotonically increasing function of the density. On the contrary, there is a mechanical instability for the Maxwell case that is initiated by the central densities for which the pressure remains constant. Such an unstable region is absent when the phase transition is treated using Gibbs' conditions. It turns out that the value of the maximum mass of neutron stars with kaon condensation is only slightly affected by the Gibbs construction[25], which is still affected by many theoretical uncertainties [55]. Therefore we limit ourselves to the Maxwell construction. In Fig.5, the region of constant pressure (thin solid line) is comprised between two values of the baryon density, denoted by $\rho_1$ and $\rho_2$. If the magnitude of $|a_3 m_s|$ is large, it may happen that $\rho_1 < \rho_0$. As a rule, we consider this solution as unrealistic, and we do not show the corresponding curve in Fig.5. This is the case when $a_3 m_s = -310$ MeV and neutrinos are trapped, that is to say that the kaon condensation requires a very stiff symmetry energy if the kaon-nucleon interaction is strongly attractive.

Once the EOS has been determined, the TOV equations can be solved. The resulting gravitational mass is plotted for neutrino free matter in Fig.6, as a function of both radius and central density, normalized with respect to the saturation value. In particular, microscopic TBF's produce stiffer equations of state, and therefore give rise to larger values of the maximum mass. We observe a decrease of the maximum mass when kaons appear, the exact value being dependent on the chosen TBF's and the parameter $a_3 m_s$. In the microscopic case, the inclusion of kaons decreases the maximum mass configuration down to about 2 $M_\odot$. On the other hand, phenomenological TBF's produce softer equations of state and, consequently, smaller neutron stars, whose maximum mass is about 1.7 $M_\odot$. In Fig.6 circles represent unstable configurations, originating from the Maxwell construction. Those configurations turn out to be stable if the Gibbs construction [25, 54] is applied to the transition from purely nuclear matter to the kaon condensed phase.

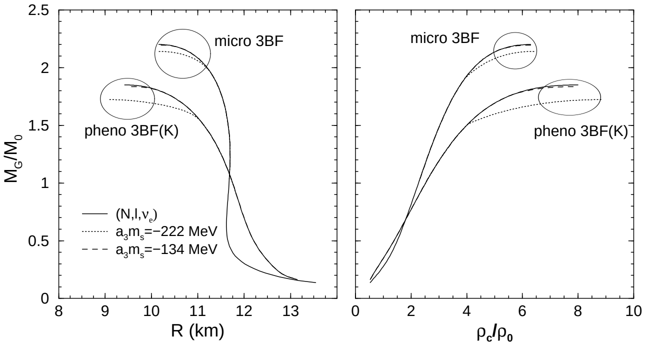

FIG. 7: The gravitational mass is shown as a function of the radius (left-hand side) and the normalized central density (right hand side), for the phenomenological (lower curves) and microscopic TBF's (upper curves) in neutrino trapped matter.

In the purely nucleonic case, neutrino trapping generally produces a softer equation of state, because beta-stable matter turns out to be more symmetric in neutrons and protons. As a consequence, the maximum mass becomes smaller. This is displayed in Fig.7. However, the appearance of kaons changes this general picture and the equation of state becomes stiffer. This is due to the fact that the $K^-$ onset depends on the lepton chemical potential, i.e., $\mu_e - \mu_{\nu_e}$, which stays at larger values in neutrino-trapped matter than in the neutrino-free case, thus delaying the appearance of $K^-$ to higher baryon density. The resulting maximum mass increases, as shown in Fig.7. If phenomenological TBF's are used, the value of the maximum mass stabilizes around 1.8 $M_\odot$, whereas microscopic TBF's give rise to protoneutron stars with mass slightly larger than 2 $M_\odot$. As compared to the neutrino free case (Fig.6), the reduction of the maximum mass due to the presence of kaons is smaller in the neutrino trapped case.

## V. SUMMARY AND CONCLUSIONS

In summary, we have investigated the properties of kaon condensed neutrino-free and neutrino-trapped matter at zero temperature including the composition, the equation of state, and the radius-mass relation, in the framework of the BHF approach with both microscopic and phenomenological three-body forces. In particular, we have discussed the interplay among the effects of the different TBFs, kaon condensate, and neutrino trapping. It is found that the effect of the microscopic TBF results in larger values of symmetry energy at high densities ($\rho_B \geq 0.4$ fm$^{-3}$ ) than that of the phenomenological one. This gives rise to a higher proton population in NS matter without neutrinos and kaons, thus allowing for fast cooling through the direct URCA process. The contribution of trapped neutrinos makes the electron concentration keep high in $\beta$-equilibrated star matter and weakens the role played by the symmetry energy on the predicted composition of the star. As a result, the composition of the star matter becomes less sensitive to the two different three-body forces considered when neutrinos are trapped.

In the star matter without kaons, neutrino trapping leads to a softening of the equation of state. However when kaons are allowed, neutrino trapping makes the equation of state stiffer as compared to the neutrino free star matter, since the presence of trapped neutrinos shifts the onset of kaons to higher densities and reduces the kaon abundance.

In both cases with and without kaons, the microscopic TBF leads to larger values of the maximum star masses than the phenomenological one. If only nucleons and leptons are allowed, the effect of neutrino trapping is to reduce the maximum star mass; while when kaons are allowed, trapping instead produces larger stars. As expected, the effect of kaon condensate is generally to soften the equation of state and reduce the predicted maximum star mass. Neutrino trapping weakens the role of kaons by delaying their onset densities to higher values and by reducing the kaon abundance. As a result, the reduction of the maximum mass due to kaon condensate is less in the neutrino trapped case than in the neutrino free case.

This general scenario could change if we include hyperons in our calculations. Several studies have been performed on hyperonic matter within the BHF approach [56, 57], showing that $\Sigma^-$ appear already at a very low value of the baryon density, i.e., $\rho_B \approx (2-3)\rho_0$. Therefore, hyperon onset might be a process in competition with kaon condensation [1], as found in relativistic mean-field approaches [51, 52, 58]. We will present a more detailed study in a forthcoming publication.

## VI. ACKNOWLEDGMENTS

One of us (W. Zuo) acknowledges the warm hospitality he received at LNS-INFN, Catania where this work started. The work was done within the Asia-Link project (CN/ASIA-LINK/008(94791)) of the European Commission. The work of A. Li and W. Zuo was supported in part by the National Natural Science Foundation of China (10575119, 10235030), the Knowledge Innovative Project of CAS (KJCX2-SW-N02), the Major Prophase Research Project of Fundamental Research of the Ministry of Science and Technology of China (2002CCB00200), the Chinese Major State Basic Research Development Program (G2000077400), and the Knowledge Innovative Project of CAS (KJCX2-SW-N02).

---

[1] M. Prakash, I. Bombaci, M. Prakash, P. J. Ellis, R. Knorren, and J. M. Lattimer, Phys. Rep. **280**, 1 (1997) and references therein.

[2] J. A. Pons, S. Reddy, M. Prakash, J. M. Lattimer, and J.A. Miralles, Astrophys. J. **513**, 780 (1999).

[3] J. A. Pons, A. W. Steiner, M. Prakash, and J. M. Lattimer, Phys. Rev. Lett. **86**, 5223 (2001).

[4] I. Vidaña, I. Bombaci, A. Polls, and A. Ramos, Astronomy & Astrophysics **399**, 687 (2003); Nucl. Phys. **A719**, 173c (2003).

[5] A. M. S. Santos, and D. P. Menezes, Phys. Rev. **C69**, 045803 (2004).

[6] P. K. Panda, D. P. Menezes, and C. Providencia, Phys. Rev. **C69**, 025207 (2005).

[7] O. E. Nicotra, M. Baldo, G. F. Burgio, and H.-J. Schulze, Astronomy & Astrophysics **451**, 213 (2006).

[8] M. Prakash, T. L. Ainsworth, and J. M. Lattimer, Phys. Rev. Lett. **61**, 2518 (1988).

[9] N. K. Glendenning, Astrophys. J. **293**, 470 (1985).

[10] J. D. Walecka, Ann. Phys. (N.Y.) **83**, 491 (1974); B. D. Serot and J. D. Walecka, Adv. Nucl. Phys. **16**, 1 (1986); Int. Journ. Mod. Phys. **E6**, 515 (1997).

[11] D. B. Kaplan and A. E. Nelson, Phys. Lett. **B175**, 57 (1986).

[12] C. H. Lee, Phys. Rep. **275**, 255 (1996) and references therein; C. H. Lee, G. E. Brown, D. P. Min, and M. Rho, Nucl. Phys. **A585**, 401 (1995).

[13] G. Q. Li, C.-H. Lee, and G. E. Brown, Phys. Rev. Lett. **79**, 5214 (1997).

[14] G. E. Brown, C.-H.Lee, and R. Rapp, Nucl. Phys. **A639**, 455c (1998).

[15] T. Muto, Progress of Theoretical Physics Supplement **153**, 174 (2004).

[16] V. Thorsson, M. Prakash, and J. M. Lattimer, Nucl. Phys. **A572**, 693(1994); **A574**, 851 (1994), Erratum.

[17] J. A. Pons, S. Reddy, J. Ellis, M. Prakash, and J. M. Lattimer, Phys. Rev. **C62**, 035803 (2000).

[18] S. Pal, D. Bandyopadhyay, and W. Greiner, Nucl. Phys. **A674**, 553 (2000).

[19] S. Banik, and D. Bandyopadhyay, Phys. Rev. **C63**, 035802 (2001).

[20] G. E. Brown, K. Kubodera, D. Page, and P. Pizzochero, Phys. Rev. **D37**, 2042 (1988).

[21] T. Tatsumi, Progress of Theoretical Physics **80**, 22 (1988).

[22] H. Fujii, T. Muto, T. Tatsumi, and R. Tamagaki, Phys. Rev. **C50**, 3140 (1994); Nucl. Phys. **A571**, 758 (1994).

[23] S. Kubis and M. Kutschera, Nucl. Phys. **A720**, 189 (2003).

[24] J. A. Pons, AJ. Miralles, M. Prakash, and J. M. Lattimer, Astrophys. J. **553**, 382 (2001).

[25] N. K. Glendenning and J. Schaffner-Bielich, Phys. Rev. Lett. **81**, 4564 (1998); Phys. Rev. **C60**, 025803 (1999).

[26] X. R. Zhou, G. F. Burgio, U. Lombardo, H.-J. Schulze, and W. Zuo, Phys. Rev. **C69**, 018801 (2004).

[27] W. Zuo, A. Li, Z. H. Li, and U. Lombardo, Phys. Rev. **C70**, 055802 (2004).

[28] T. Tatsumi, and M. Yasuhira, Phys. Lett. B **441**, 9 (1998); Nucl. Phys. **A670**, 218c (2000).

[29] T. Muto, T. Tatsumi, and N. Ywamoto, Phys. Rev. D **61**, 063001 (2000); **61**, 083002 (2000).

[30] A. Li, G. F. Burgio, U. Lombardo, and W. Zuo, in preparation.

[31] I. Bombaci, and U. Lombardo, Phys. Rev. **C44**, 1892 (1991).

[32] W. Zuo, I. Bombaci, and U. Lombardo, Phys. Rev. **C60**,

024605 (1999).

[33] J.P. Jeukenne, A. Lejeune and C. Mahaux, Phys. Rep. **25**, 83 (1976).

[34] H. Q. Song, M. Baldo, G. Giansiracusa, and U. Lombardo, Phys. Rev. Lett. **81**, 1584 (1998); M. Baldo, A. Fiasconaro, H. Q. Song, G. Giansiracusa, and U. Lombardo, Phys. Rev. **C65**, 017303 (2002).

[35] R. B. Wiringa, V. G. J. Stoks, and R. Schiavilla, Phys. Rev. **C51**, 38 (1995).

[36] M. Baldo, I. Bombaci, and G. F. Burgio, Astron. Astrophys. **328**, 274 (1997).

[37] B. S. Pudliner, V. R.Pandharipande, J. Carlson, and R. B. Wiringa, Phys. Rev. Lett. **74**, 4396 (1995); B. S. Pudliner, V. R.Pandharipande, J. Carlson, S. C. Pieper, and R. B. Wiringa, Phys. Rev. **C56**, 1720 (1997).

[38] P. Grangé, A. Lejeune, M. Martzolff, and J.-F. Mathiot, Phys. Rev. **C40**, 1040 (1989).

[39] A. Lejeune, U. Lombardo, and W. Zuo, Phys. Lett. **B477**, 45 (2000); W. Zuo, A. Lejeune, U. Lombardo, and J.-F. Mathiot, Eur. Phys. J **A14**, 469 (2002).

[40] S. L. Shapiro, and S. A. Teukosky, *Black Holes, White Dwarfs, and Neutron Stars*, (John Wiley, New York, 1983).

[41] G. E. Brown, K. Kubodera, M. Rho, and V. Thorsson, Phys. Lett. **B291**, 355 (1992).

[42] H. D. Politzer and M. B. Wise, Phys. Lett. **B273**, 156 (1991).

[43] J. F. Donoghue and C. R. Nappi, Phys. Lett. **B168**, 105 (1986).

[44] S. J. Dong, J.-F. Lagaë, K. F. Liu, Phys. Rev. **D54**, 5496 (1996).

[45] G. Baym , Phys. Rev. Lett. **30**, 1340 (1973).

[46] R. C. Tolman, Phys. Rev. **55**, 364 (1939).

[47] J. R. Oppenheimer and G. M. Volkoff, Phys. Rev. **55**, 374 (1939).

[48] J. W. Negele, and D. Vautherin, Nucl. Phys. **A207**, 298 (1973).

[49] R. Feynman, F. Metropolis, and E. Teller, Phys. Rev. **75**, 1561 (1949).

[50] G. Baym, C. Pethick, and D. Sutherland, Astrophys. J. **170**, 299 (1971).

[51] R. Knorren, M. Prakash, and P. J. Ellis, Phys. Rev. **C52**, 3470(1995).

[52] J. Schaffner, and I. N. Mishustin, Phys. Rev. **C53**, 1416(1996).

[53] A. B. Migdal, in: Mesons in Nuclei, vol.3, eds. M. Rho and D. Wilkinson (North-Holland, Amsterdam, 1979)

[54] N. K. Glendenning, Phys. Rev. **D46**, 1274(1992).

[55] T. Maruyama, T. Tatsumi, D. N. Voskresensky, T. Tanigawa, T. Endo, and S. Chiba, Phys. Rev. **C73**, 035802 (2006).

[56] M. Baldo, G. F. Burgio, and H.-J. Schulze, Phys. Rev. **C58**, 3688(1998); Phys. Rev. **C61**, 055801(2000).

[57] I. Vidaña, A. Polls, A. Ramos, L. Engvik, and M. Hjorth-Jensen, Phys. Rev. **C62**, 035801(2000).

[58] P. J. Ellis, R. Knorren, and M. Prakash, Phys. Lett. **B349**, 11(1995).